

Three-dimensional co-culturing of stem cell-derived cardiomyocytes and cardiac fibroblasts reveals a role for both cell types in Marfan-related cardiomyopathy

Jeffrey Aalders^a, Laurens Léger^a, Louis Van der Meeren^b, Sanjay Sinha^c, Andre G. Skirtach^b, Julie De Backer^{d,e} and Jolanda van Hengel^{a*}

Affiliations

- a. Medical Cell Biology Research Group, Department of Human Structure and Repair, Faculty of Medicine and Health Sciences, Ghent University, Ghent, Belgium.
- b. Department of Biotechnology, Faculty of Bioscience Engineering, Ghent University, Ghent, Belgium.
- c. Wellcome-MRC Cambridge Stem Cell Institute, University of Cambridge, Cambridge, UK.
- d. Centre for Medical Genetics, Ghent University Hospital, Belgium and Department of Biomolecular Medicine, Ghent University, Ghent, Belgium.
- e. Department of Cardiology, Ghent University Hospital, Ghent, Belgium.

*Corresponding author: Jolanda.vanHengel@Ugent.be

Highlights

- Cardiac fibroblast and cardiomyocytes play a role in Marfan-related cardiomyopathy.
- Abnormal early cardiac development may lead to Marfan-related cardiomyopathy.
- Marfan cardiac fibroblasts show disturbed cell-cell and cell-matrix interactions.

Abstract

Pathogenic variants in the *FBN1* gene, which encodes the extracellular matrix protein fibrillin-1, cause Marfan syndrome (MFS), which affects multiple organ systems, including the cardiovascular system. Myocardial dysfunction has been observed in a subset of patients with MFS and in several MFS mouse models. However, there is limited understanding of the intrinsic consequences of *FBN1* variants on cardiomyocytes (CMs). To elucidate the CM-specific contribution in Marfan's cardiomyopathy, cardiosphere cultures of CMs and cardiac fibroblasts (CFs) are used. CMs and CFs were derived by human induced pluripotent stem cell (iPSC) differentiation from MFS iPSCs with a pathogenic variant in *FBN1* (c.3725G>A; p.Cys1242Tyr) and the corresponding CRISPR-corrected iPSC line (Cor).

Cardiospheres containing MFS CMs show decreased *FBN1*, *COL1A2* and *GJA1* expression. MFS CMs cultured in cardiospheres have fewer binucleated CMs in comparison with Cor CMs. 13% of MFS CMs in cardiospheres are binucleated and 15% and 16% in cardiospheres that contain co-cultures with respectively MFS CFs and Cor CFs, compared to Cor CMs, that revealed up to 23% binucleation when co-cultured with CFs. The sarcomere length of CMs, as a marker of development, is significantly increased in MFS CMs interacting with Cor CF or MFS CF, as compared to monocultured MFS CMs.

Nuclear blebbing was significantly more frequent in MFS CFs, which correlated with increased stiffness of the nuclear area compared to Cor CFs.

Our cardiosphere model for Marfan-related cardiomyopathy identified a contribution of CFs in Marfan-related cardiomyopathy and suggests that abnormal early development of CMs may play a role in the disease mechanism.

Keywords

Marfan syndrome, fibrillin-1, cardiomyocytes, cardiac fibroblasts, disease modelling, extracellular matrix

Introduction

Fibrillin-1 is a large glycoprotein of 350 kDa that can self-assemble into microfibrils and is an important component of the extracellular matrix (ECM) of elastic tissues, providing both structure and support [1]. It is also an important regulator of the bioavailability of circulating TGF β , as it plays an important part in sequestering TGF β in the latent form through latent TGF β binding proteins. Fibrillin-1 also plays a key role in mechanosignalling functions [2]. Pathogenic variants in *FBN1*, the gene encoding fibrillin-1, cause Marfan syndrome (MFS). To date, more than 3000 different pathogenic variants have been described in *FBN1*, with difficult-to-predict genotype-phenotype correlations [3]. MFS is an ECM disease and affects multiple organ systems, including the cardiovascular, ocular, skeletal, integumentary, and respiratory organ systems [4]. The most common complication in patients with MFS involves aortic root dilatation, leading to potential aneurysm, dissection, and rupture. Improved clinical management in MFS has resulted in increased life expectancy [5]. Other reported clinical manifestations causing mortality and morbidity in patients with MFS include myocardial dysfunction and sudden cardiac death independent from aortic or valvular disease. This raises the concept of an intrinsic, or primary cardiomyopathy, named MFS-related cardiomyopathy [6].

While myocardial dysfunction has been reported in several independent cohorts of patients with MFS [6-8] and in several MFS mouse models [9], little is known about the intrinsic consequences of the *FBN1* variants on the cardiomyocytes (CMs) and the mechanisms leading to primary Marfan-related cardiomyopathy. Previously, we have reported the first *in vitro* myocardial model for MFS using CMs differentiated from human induced pluripotent stem cells (iPSCs) [10]. Functional analysis of the 2D cultures was performed by atomic force microscopy (AFM), multi-electrode array (MEA) and cell stretching (Flexcell), revealing abnormalities in the CMs with a Marfan phenotype. MFS CMs showed a lower beat-to-beat variability, were stiffer and received incomplete matrix support in contrast to corrected (Cor) CMs. These functional abnormalities of the MFS CMs underline the significant contribution of impaired fibrillin-1 in the ECM.

CMs and cardiac fibroblasts (CFs) attribute to the cardiac ECM [11], but their relative role in MFS-related cardiomyopathy is unknown. The interplay between the various cells and the extracellular matrix is essential for normal cardiac development. With CFs in the microenvironment, nutrients, growth factors and biophysical cues are exchanged. Despite only making up 18-30% of the total cell number in the adult heart, CMs are responsible for 80% of the volume [12, 13]. During the postnatal cardiac development, the number of CMs remain constant while the number of mesenchymal and endothelial cells increase up to young adulthood, resulting in decreasing percentage of CMs in the heart [13].

2D cultures of iPSC-derived CMs are useful for disease modelling purposes, however, it is accompanied by numerous constraints, including disruptions to the interactions between cellular and extracellular environments and alterations in cell morphology. Currently, several methods have been optimized for 3D culturing of CMs. iPSC-derived CMs casted in fibrin-based engineered heart tissues are arguably the most mature CMs obtained in *in vitro* cultures [14]. An attractive alternative is scaffold-free self-assembly of CMs in low-attachment dishes into 3D structures. These culture systems increase cell interactions and provide a suitable technique to study multi-cellular *in vitro* cultures. Various names have been used to address these 3D structures, for example cardiac microtissues [15], cardiospheres [16] and cardiac spheroids [17]. To decipher the CM-specific contribution, we employed cardiospheres composed of CMs and CFs, further advancing our previously published MFS myocardial model [10].

Combining the data from our previous 2D *in vitro* model with our cardiosphere model suggests that abnormal early development of CMs because of disturbed cell-matrix interactions and dysregulated direct cell-cell communication with CFs may lead to MFS-related cardiomyopathy.

Results

CMs and quiescent CFs (**Suppl Fig 1**) were derived from a patient with MFS with a *FBN1* pathogenic missense variant (c.3725G>A; p.Cys1242Tyr – named *FBN1* variant from here on) and Cor iPSCs to create a cardiosphere model for Marfan-related cardiomyopathy and to decipher the role of CMs and CFs in the disease mechanism in a mixed cardiosphere model. This pathogenic variant models a dominant negative effect as demonstrated previously by similar *FBN1* expression in 2D CMs [10] and smooth muscle cells [18]. The study design is depicted in **Fig 1**. The findings of this study include a decreased percentage of binucleated cardiomyocytes and decreased sarcomere length in Marfan compared to corrected cardiosphere cultures.

Similar size and shape of mixed cardiospheres

While the cardiospheres in all conditions consist of an equal number of cells (20.000), the cell type composition and source (Cor or MFS) were different. To test if floating cardiosphere formation is

affected by the *FBN1* variant, CMs and CFs were co-cultured and compared to cardiospheres that consist only of CMs. Cardiosphere formation was successful and reproducible in all conditions, resulting in beating structures after a recovery period of approximately 2 days. First, cardiospheres were analysed to establish the relevant culture time. After 21 days of culture MFS cardiospheres had significant larger diameter compared to Cor cardiospheres (**Fig 2A, B**). While the interaction with CFs shows impact on cardiosphere size in the first week of cardiosphere culture, it had no impact on final cardiosphere size at day 21. Dysregulated gene expression for *FBN1* and *GJA1* was observed in 7 day- and 14 day-old cardiospheres when comparing Marfan with corrected (**Fig 2C**). Maturation marker *TNNI3/TNNI1* was upregulated in 21 day-old cardiospheres compared to earlier timepoints. Based on this data 7 day-old cardiospheres were selected as most suitable to investigate abnormalities in early development in Marfan-related cardiomyopathy. No significant difference in size was observed between any of the conditions at day 7 (**Fig 2D**). To further investigate the size difference between MFS and corrected cardiospheres at later timepoints the possibility of increased compaction or alternatively dilation was explored. However, mean fluorescent intensity of Hoechst signal was not significantly different in the cardiospheres (**Fig 2E**). Total cell numbers were estimated using integrated density of the Hoechst signal, which reveals a significant increase for MFS cardiospheres at day 3, 14 and 21. This implies that the increased size of MFS cardiospheres could be explained by increased cellular proliferation as a result of impaired fibrillin-1.

Transcription profiles for FBN1, GJA1, MLC2v, MLC2a, ITGB1 and COL1A2 in cardiospheres are modulated by the pathogenic variant in FBN1

Gene expression analysis using RT-qPCR was performed to see how the interaction between CMs, CFs and the *FBN1* variant affect the transcriptional profile of the cardiospheres (**Fig 3**). Both CMs and CFs contribute to the overall gene expression in co-culture conditions. While CMs are the predominant cell type (17.000 cells) in the cardiosphere co-cultures compared to the CFs (3000 cells), the relative contribution of CMs and CFs to the total gene expression observed is unknown. Therefore, the gene expression profiles can be compared with pure cardiosphere culture consisting of only CMs (20.000 cells). A higher expression observed in mixed cardiospheres compared to cardiospheres with only CMs indicates that either the target gene is more expressed by CFs, or that CMs become more transcriptionally active via CM-CF interactions.

Overall, *FBN1* expression decreased two-fold in cardiosphere cultures with MFS CMs (**Fig 3**). The expression for *GJA1*, coding for connexin-43, was significantly lower in cardiospheres with MFS CMs compared to cardiospheres with Cor CMs. The expression for *MLC2v*, a ventricular cardiac muscle form of myosin light chain 2, was significantly higher in cardiospheres with MFS CMs compared to cardiospheres without MFS CMs. *MLC2a* expression shows a similar expression profile as *MLC2v*,

where *MLC2a* expression was significantly higher in cardiospheres with MFS CMs compared to cultures with Cor CMs. *ITGB1* expression, coding for integrin $\beta 1$ was significantly upregulated in mixed cardiospheres with MFS CFs compared to cardiospheres with only CMs. Expression of *COL1A2*, coding for collagen type 1, was significantly lower in conditions with MFS CMs, compared to Cor CMs. *TNNT2* does not show significant difference in expression across the conditions. Lastly, the *TNNI3/TNNI1* ratio, which is an indicator of CM maturation was not significantly different between the different cardiospheres.

Connexin-43 is localized on the cell-cell borders between cardiac fibroblasts and cardiomyocytes

Immunohistochemical analysis for connexin-43 was performed on cells that underwent 3D culture and were left to attach and form a monolayer. Connexin-43 was localized at the cell-cell borders between CMs where they are involved in the conduction. Connexin-43 in CFs was mainly localized at the location of the cell membrane. No differences in abundance of connexin-43 and α -actinin at the cell border was observed between any of the cardiosphere conditions of Cor and MFS (**Fig 4C**). The presence of connexin-43 at the cell-cell contacts between CFs and CMs suggest an interaction between the two cells. Connexin-43 was not exclusively localized at the junctional area but was also present in the perinuclear area. This indicates incomplete migration of connexin-43 to the plasma membrane, which could be due to a lack of cell maturation. Quantification of total connexin-43 abundance revealed no increase in cardiospheres with Cor CMs compared to cardiospheres with MFS CMs besides Cor CM + MFS CF at day 7 and day 14 (**Suppl Fig 2**). In addition, cell-cell interactions via cadherins and β -catenin between CMs were observed in both Cor and MFS conditions (**Fig 4A, B**). Moreover, quantification revealed no dysregulated abundance of N-cadherin (**Suppl Fig 3**) and β -catenin (**Suppl Fig 4**).

Sarcomere length of Marfan cardiomyocytes increases when co-cultured with cardiac fibroblasts

Sarcomere length was evaluated to assess if CMs undergo structural changes when co-cultured with CFs. This length is defined as the distance between two consecutive Z-lines, which are stained using α -actinin (**Fig 5A**). The immunohistochemical analysis was performed on cells that underwent 3D culture and were left to attach and form a monolayer. No significant increase of sarcomere length was observed for Cor CMs that are co-cultured with Cor CFs or MFS CFs (**Fig 5B**). In case of MFS CMs, a significant increase was observed when co-cultured with either MFS CFs or Cor CFs.

Nucleation status of Marfan cardiomyocytes reveals a lower percentage of binucleated cardiomyocytes

The nucleation status of CMs was analysed to see if co-culture with CFs could result in structural changes in CMs. Binucleated CMs are characterized by two equally sized nuclei in one single CMs, in

contrast to mononucleated CMs that have only one nucleus (**Fig 5C, D**). In order to quantify the number of nuclei per CM, cardiospheres were dissociated and seeded in 2D on Geltrex-coated coverslips. A significant increase in the percentage of binucleated CMs was observed for Cor CMs when co-cultured with MFS CFs and Cor CFs (**Fig 5E**). Cor CMs reached a percentage of over 23% binucleated CMs when co-cultured with Cor CFs, this was significantly higher than MFS CMs that are co-cultured with Cor CFs (only reaching 16.5%, which is similar as 16.6% of Cor CMs only).

Nuclear blebbing occurs more frequently in Marfan cardiac fibroblasts

The structure of the nucleus was assessed in 2D monolayers of CMs and CFs using immunohistochemical analysis for Lamin A/C, which stains the nuclear lamina. **Fig 5F** shows Cor CFs with normal nuclear shape and MFS CFs with nuclear blebs, as indicated by the arrow. Also, CMs with nuclear blebbing were observed (**Fig 5G**). Quantifying the nuclei with blebs revealed a low percentage in CMs (approximately 5%) and revealed no differences between Cor CMs and MFS CMs (**Fig 5H**). However, when comparing the percentage of nuclear blebs in CFs, a significant increase in MFS CFs (21%) was observed compared to Cor CFs (2%) and remarkably higher than in CMs.

Atomic force microscopy reveals increased stiffness of the perinuclear area of Marfan cardiac fibroblasts

AFM was used to measure subcellular differences in stiffness in 2D monolayers of CFs. A clear cellular region can be observed in CFs, being the area on and around the nucleus, the perinuclear area, a region located higher and with a blue colour (meaning lower Young's modulus) indicated by the yellow arrows in **Fig 5I**. The average Young's modulus for the perinuclear region was significantly higher in MFS CFs (7.9 kPa) compared to Cor CFs (3.4 kPa, **Fig 5J**), this can also be noted on the 3D Young's modulus images, the perinuclear area of Cor CFs appears to be darker blue compared to MFS CFs (**Fig 5I**).

Discussion

In this study we describe our investigation of the first human *in vitro* cardiosphere model for Marfan-related cardiomyopathy consisting of CMs or a mixed cardiosphere model consisting of CMs and CFs (**Fig 1**). In our previous study we reported an *in vitro* 2D monolayer culture of CMs for Marfan-related cardiomyopathy that displayed abnormal behaviour in MFS CMs [10]. Advances in *in vitro* 3D culture have allowed researchers to decipher the involvement of specific cell types and disease mechanisms in more detail whilst maintaining an *in vivo*-like cell environment. CMs in cardiospheres display improved maturation demonstrated by increased sarcomere length [19]. Cardiospheres have been used to model various cardiomyopathies, including arrhythmogenic cardiomyopathy, revealing that CFs carrying a pathogenic variant for arrhythmogenic cardiomyopathy affect healthy CMs, resulting in

arrhythmia [20]. This highlights the importance of the interplay between the various cell types of the heart. Both 3D culturing and co-culturing with CFs are established interventions to increase maturity in CMs, and the combination of both is thought to further increase maturation.

The cardiospheres generated in this present study displayed good reproducibility suitable for medium through-put analysis, demonstrating the low-attachment 96-well plates as a successful strategy for disease modelling. The generated 7 day-old cardiospheres in this study have an approximate diameter of 500 μm for 20,000 cells (**Fig 2D**) which is in accordance with previous studies using CMs in 3D self-assembled structures that used 5,000 cells and measured 400 μm cardiospheres [17, 20] and another study using 50,000 cells per cardiosphere that reported diameters of approximately 500 μm [21]. Another study using co-cultures of CMs and non-CMs (cells identified as non-CMs after cardiac differentiation) derived from hiPSCs showed the best electrophysiological properties in co-cultures with 70-90% CMs [22]. Our study used 85% CMs, similarly to Giacomelli *et al* 2020 [20].

Interestingly, 21 day-old MFS cardiospheres display increased size compared to corrected cardiospheres (**Fig 2B**). As expected older cardiospheres also revealed increased maturation compared to younger cardiospheres (**Fig 2C**). Notably, in 21 day-old cardiospheres the gene expression for *GJA1* was normalized compared to earlier timepoints in which *GJA1* was dysregulated. Although dilated cardiomyopathy is observed in MFS [23], no evidence was found for this to explain size differences in the cardiosphere model (**Fig 2E**). Instead, increased cellular proliferation may be hypothesized as the contributing factor to the observed size differences in the cardiospheres (**Fig 2F**). Generally proliferation rate of CMs decreases with maturation. This finding fits in the overall hypothesis that delayed or abnormal early development results in Marfan-related cardiomyopathy.

Gene expression was evaluated for various ECM and cardiac-related genes. For *FBN1*, a significant decrease in gene expression is observed in cardiospheres with MFS CMs (**Fig 3**). Our previously published 2D *in vitro* model displayed a significantly increased *FBN1* expression from d15 to d24 in MFS CMs, compared to a steady-state *FBN1* gene expression at d15 and d24 in Cor CMs [10]. Here, the observed difference between cardiospheres with MFS CMs could be explained by the cardiospheres' reliance on the native cell-produced matrix for self-assembly, in contrast to 2D monolayer cultures where Geltrex was provided. This is further evidenced by another matrix protein, *COL1A2*, that shows a significant increase in expression in cardiospheres with Cor CMs, similarly to *FBN1* expression. Integrins mediate binding to fibrillin-1, impaired interactions with fibrillin-1 in MFS may lead to a compensatory effect by increasing integrin $\beta 1$ expression to facilitate binding, which could explain the significant increase of integrin $\beta 1$ in cardiospheres containing MFS CFs.

CFs function as suppliers of cyclic guanosine monophosphate (cGMP), which is transported to cardiomyocytes CMs through gap junctions. This cGMP, in turn, hinders the function of phosphodiesterases (PDEs) responsible for the conversion of cAMP to AMP and contributes to maturation in CMs [20]. *GJA1*, which encodes for connexin-43, an important gap junction protein, shows a significant decrease in expression in cardiospheres with MFS CMs (**Fig 3**). Decreased *GJA1* gene expression could result in reduced gap junction formation, leading to impaired cell-cell communication between CMs and CFs [24, 25]. Moreover, dysregulated hemichannels could also contribute to cardiac dysfunction [26]. Part of the connexin-43 localizes in the perinuclear area, probably due to the relative level of maturity of the cells in our models compared to the *in vivo* human heart. This could explain why no remarkable differences in morphology or quantity of these junctions between CMs and CFs was observed in MFS based on immunohistochemical analysis (**Fig 4**). Further improving maturation of the cells would be a prerequisite to determine effects on protein localization and potential abnormalities in MFS. Connexin-43 is known for its role as a membrane protein, however, various truncated isoforms have been described in the human heart, playing important roles in the autoregulation of connexin-43 [27]. The imbalance of full length and truncated isoforms may explain the differences observed in *GJA1* expression between MFS and Cor. Another possibility, next to homotypic connexin-43 gap junctions, could be that heterotypic gap junctions (connexin-43 and connexin-45) are formed between CMs and CFs which are also involved in cardiac function [28, 29] and may explain the observed differences in MFS and Cor. The upregulation of cardiac specific genes *MLC2v* and *MLC2a* in MFS may point to an adaptive response of the CMs. These two markers coincide with sub specification of CMs, respectively ventricular and atrial. Since both *MLC2v* and *MLC2a* increase in MFS CMs, no clear sub specification was identified. The *TNNI3/TNNI1* ratio is considered a marker of maturation in CMs, with higher values pointing to increased maturation [30]. The gene expression pattern observed in the cardiospheres suggests that co-culturing with CFs may enhance maturation of CMs.

Analysis of the CMs from cardiospheres shows that interaction with CFs can modulate CM properties. The main findings of this study are that pathogenic *FBN1* variants affect development of CMs as demonstrated by two developmental markers: sarcomere length and binucleation in CMs. Sarcomere length was shorter in MFS CMs compared to Cor CMs, however not significantly (**Fig 5B**). Improvement of sarcomere length by 3D co-culturing with CFs is also described previously [20]. Interestingly, we found that the sarcomere length of MFS CMs was significantly increased by co-culturing with Cor CFs or MFS CFs, reaching similar sarcomere lengths as Cor CMs. Another hallmark of development is the binucleation in CMs. The proliferative capacity of the human adult heart is limited, this coincides with cell-cycle exit by either failed karyokinesis (resulting in polyploidy) or failed cytokinesis, which results

in multinucleation [13]. The percentage of binucleated CMs is thus a measure that coincides with development. In human adult heart tissue, the percentage of binucleated CMs is estimated at approximately 25% of the CMs [13]. Co-culturing of CMs with CFs increases the percentage of binucleated CMs, however only significant for Cor CMs (**Fig 5E**). Interestingly, co-culturing Cor CMs with Cor CFs resulted in more than 23% binucleated CMs, which is comparable to the human adult heart. The increase of binucleation in MFS CMs was limited and only reached similar levels as Cor CMs without co-culture (16%). These findings pose the idea of delayed development in MFS CMs but also reveals the role for CFs in modulating CMs properties.

Based on the observed differences in binucleation we subsequently studied the nucleus of the CMs and CFs more closely by immunohistochemical analysis of the nuclear membrane using Lamin A/C. Lamin A/C plays a key role in the nuclear lamina and can also regulate gene expression. Forces of the cytoskeletal network are transmitted to the nucleus by the connection with the LINC (linker of the nucleoskeleton and cytoskeleton) complexes. Mutations in *LMNA*, the gene coding for Lamin A and C isoforms result in laminopathy leading to a wide range of manifestations, including cardiac dysfunction with conduction disturbances, (supra)ventricular arrhythmias, and dilated cardiomyopathy [31, 32]. Interestingly, abnormal structures in the form of small protrusions, also called nuclear blebs were observed. While these abnormalities were observed in both CMs and CFs from MFS and Cor the quantity was different in CFs (**Fig 5H**). MFS CFs showed significantly more frequent blebbing of the nucleus compared to Cor CFs (respectively 20% vs 2%). Nuclear blebbing was reported to result in increased nuclear membrane rupture [33]. Another study also identified that chromatin histone modifications influence nuclear rigidity and could induce nuclear blebs [34], whereas Lamin A is most important in resistance against large deformations of the nucleus. Remodelling of the nuclear lamina and histone modifications can also result from TGF β 1 exposure [35]. The increased percentage of nuclear blebbing in MFS CFs could thus be explained by a response to dysregulated mechanotransduction and increased TGF β 1 levels because of impaired fibrillin-1 in the ECM.

Stiff substrates exert more external force on the nucleus, resulting in more frequent blebbing in laminopathy, however when cultured on soft substrate (3 kPa) no increased blebbing in fibroblasts with *LMNA* mutations were observed compared to control [36]. In our experiments, the CFs were cultured on glass coverslips, being a very stiff substrate, which is thought to impose increased external stress on the MFS CFs. Using AFM we were able to demonstrate that stiffness was dysregulated in the perinuclear area of MFS CFs (**Fig 5J**) which could explain the nuclear blebbing observed in MFS. These findings pose the idea for a disease mechanism in Marfan-related cardiomyopathy that acts through nuclear blebbing of CFs in response to increased stiffness of the ECM that may result in transcriptional alternations.

In this study, we investigated a cardiosphere model for Marfan-related cardiomyopathy derived from hiPSCs carrying a pathogenic variant in *FBN1* (c.3725G>A; p.Cys1242Tyr). Our model identified that both CFs and CMs play a role in Marfan-related cardiomyopathy. We postulate that abnormal early development of CMs as a consequence of disturbed cell-matrix interactions and direct cell-cell interactions with CFs may lead to MFS-related cardiomyopathy.

Experimental procedures

Ethics statement

The local ethical committee of Ghent University Hospital approved the experiments conducted with the hiPSCs (EC UZG 2017/0855).

Culture of hiPSCs

The isogenic pair consisting of Cor and MFS hiPSCs was first described and characterized by the Sinha lab [18]. The MFS hiPSC line carries a pathogenic variant in exon 30 of *FBN1* (c.3725G>A). The feeder-dependent cultures were adapted to feeder-free conditions accordingly to a previous published protocol [37]. hiPSCs were maintained in Essential 8 medium (Life Technologies, Cat No. A1517001) with 100 u/ml Penicillin and 100 µg/ml Streptomycin (Life Technologies, Cat No. 15140-122) on Geltrex coating (Life Technologies, Cat No. A1413302) at 37 °C, 5% CO₂ and 5% O₂. For routine culture of hiPSCs enzymatic passaging was performed by incubating the cells for 3-5 min with TrypLE select (Life Technologies, Cat No. 12563011). After inactivation of TrypLE by diluting with Essential 8 medium, cell suspension was centrifuged at 200g for 5 min. Essential 8 medium with 1:100 RevitaCell (Life Technologies, Cat No. A2644501) was used to dissolve the pellet. The cell suspension was subsequently seeded with a density of 2.1×10^4 cells/cm². Image acquisition was performed with EVOS™ XL Core Cell Imaging System.

Differentiation and culturing of hiPSC derived cardiomyocytes

Differentiation of CMs from hiPSCs was performed using a directed differentiation protocol based on the modulation of Wnt [38]. The differentiation was initiated when hiPSC cultures reached a confluency of approximately 70%. First, hiPSCs were washed with PBS and then the medium was changed to differentiation medium containing 4 µM CHIR99021 (Merck, Cat No. 361559). The differentiation medium consists of RPMI 1640 with HEPES (5958 mg/l) and GlutaMAX (L-Alanyl-Glutamine 446 mg/l) (Life Technologies, Cat No. 72400-021) supplemented with 0.125 mg/ml Albumin (Sigma-Aldrich, Cat No. A9731) and 0.05 mg/ml L-Ascorbic Acid 2-Phosphate (Sigma-Aldrich, Cat No. A8960). Exactly 48h after the start of differentiation, the medium was changed by first washing the cells once with PBS and then adding differentiation medium containing 5 µM IWP2 (Merck, Cat No. 681671). On day 4 and day 6 the medium was changed to fresh differentiation medium. From day 8

onward the medium was refreshed with cardio maintenance medium every other day. Cardio maintenance medium consists of RPMI 1640 with HEPES and GlutaMAX supplemented with 1:100 B27 with insulin (Life Technologies, Cat No. 17504-044). The differentiation was performed at 37 °C, 5% CO₂ and 5% O₂, the cells were changed to 37 °C, 5% CO₂ and 19% O₂ when the first contractions of CMs were observed (day 8-10). For the dissociation of cardiomyocytes into single cell suspension, the Multi Tissue Dissociation Kit 3 (Miltenyi Biotec, Cat No. 130-110-204) was employed following the guidelines provided by the manufacturer. CMs were washed three times with PBS and subsequently incubated at 37 °C for 10 min with the dissociation mix. CMs were dissociated by gently pipetting up and down, the dissociation enzymes were inactivated by diluting with cardio maintenance medium which was supplemented with 20% FBS (Life Technologies, Cat No. 10500-064). The cell suspension was centrifuged at 200g for 5 min, and the pellet was dissolved in cardio maintenance medium supplemented with 20% FBS and 1:100 RevitaCell.

Differentiation and culturing of hiPSC derived cardiac fibroblasts

Differentiation of hiPSCs to CFs is identical to the first 4 days of differentiation to CMs. On day 4, the cardiac progenitor cells were dissociated with TryPLE select for 5 min at 37°C and re-plated with a density of 20.000 cells/cm² in Advanced DMEM/F12 (Life Technologies, Cat No. 12634010) supplemented with 5 µM CHIR99021 and 2 µM retinoic acid (Sigma, Cat No. R2625-50MG) on Geltrex coating. On day 7, medium was changed to Advanced DMEM/F12. On day 11, the medium was changed to fibroblast growth medium (DMEM/F12 (Life Technologies, Cat No. 31330038) with 10% FBS) supplemented with 10 µM bFGF (Peprotech, Cat No. 100-18B) and 10 µM SB431542 (Selleck Chemicals, Cat No. S1067-10mg). Up until day 18, the enriched fibroblast growth medium was renewed every 2-3 days. Starting from day 18, the enriched fibroblast growth medium was changed to standard fibroblast growth medium. CFs could be dissociated for further expansion or for co-culture experiments. CFs were dissociated when a confluency of 90% was reached by incubating the cells for 5 min with TryPLE select. Cell dissociation was achieved through careful pipetting up and down. Subsequently, the resulting cell suspension was centrifuged for 5 min at 200g, followed by resuspension of the pellet in fibroblast growth medium. For expansion culture, the CFs were seeded in a passaging ratio of 1:6 to 1:8 on Geltrex coating. The fibroblast growth medium was renewed every 3 days.

3D co-culture experiment using cardiospheres

Co-cultures were created by combining 14 day-old CMs and 30 dayold CFs. The cells were dissociated as described previously. Next, dissociated cells were diluted in cardio maintenance medium supplemented with 20% FBS. Cells counting was performed using a Bürker counting chamber and suspensions were centrifuged for 5 min at 200g. The pellet was dissolved in cardio maintenance

medium with 20% FBS and 1:100 RevitaCell. Co-cultures of 20.000 cells/ 96-well were made by mixing 17.000 CMs and 3.000 CFs (ratio of 85% and 15% respectively). Different combinations of Marfan and Cor cells were made as depicted in **Fig 1**. As a control, monocultures of Cor CMs and MFS CMs were seeded at a concentration of 20.000 cells/96-well. The cells were seeded on a low-attachment 96-well plate with U-bottom (FaCellitate, Cat No. F202003). Cardiosphere formation occurred relatively fast (24h-48h) by self-assembly of CMs and CFs. After three days, half of the medium was changed daily with cardio maintenance medium. The size and circularity of the formed cardiospheres was measured from day 1 to day 21 using FIJI [39]. The diameter of the cardiospheres was calculated from the measured area. The circular shape of the cardiosphere was calculated using the circularity measurement function in FIJI. Mean intensity and integrated density of Hoechst fluorescent signal were quantified using FIJI. After 7 days, cardiospheres were collected for RNA extraction, or if mentioned otherwise. To perform immunohistochemical analysis, cardiospheres were dissociated using the Multi Tissue Dissociation Kit 3 following the guidelines provided by the manufacturer. The cell suspensions obtained from three cardiospheres were combined in cardio maintenance medium with 20% FBS and 1:100 RevitaCell. These cell suspensions were transferred to 24-wells with a glass coverslip coated with Geltrex to grow for 7 days into a monolayer.

Immunohistochemical analysis

Cells on coverslips were fixed with 4% paraformaldehyde at RT for 20 min. Permeabilization of the cells was performed with 0.1% Triton X-100 diluted in PBS for 8 min. Blocking was performed with blocking buffer, consisting of PBS with 0.05% Tween20 and 1% bovine serum albumin (BSA) for 60 min. The cells were incubated with primary antibody diluted in the blocking solution overnight at 4 °C. The antibodies used are listed in **supplementary table 1**. The next day, the cells were incubated overnight at 4 °C with the secondary antibody and 1/1000 HOECHST (Life Technologies, Cat No. H3570) diluted in blocking solution. Microscopy images were made using a ZEISS LSM900 confocal microscope or EVOS FL Imaging System. Connexin-43, cadherin and β -catenin abundance was quantified based on a previous published method [40]. The analysis is based on the fluorescent signal and determines the specific signal based on thresholding and normalizes on the background using a low threshold. Image analysis was performed using FIJI.

Gene expression analysis

5-10 cardiospheres were collected for RNA extraction. The extraction process was carried out using the GeneElute Mammalian Total RNA Miniprep kit (Sigma-Aldrich, Cat No. RTN70), which involved on-column DNA digestion as per the manufacturer's instructions. cDNA synthesis kit (Biotechrabbit, Cat No. BR0400404) was used to convert RNA to cDNA. qPCR was executed using the Platinum SYBR Green qPCR SuperMix-UDG kit (Life Technologies, Cat No. 11733038) on a CFX96 Touch Real-Time PCR

Detection System (Bio-Rad). The qPCR protocol consisted of an initial 50°C step for 2 min and a denaturation step at 95 °C for 2 min, followed by 40 cycles of amplification at 95 °C for 20 s and 60 °C for 45 s. The primers were employed at a final concentration of 200 nM and are detailed in **supplementary table 2**. Evaluation of the qPCR results was performed using the CFX Manager software (Bio-Rad). Gene expression was normalized to *B2M* and *RPL13A* using Genorm [41].

Atomic force microscopy

All AFM measurements were performed on CFs in a 2D monolayer on glass with the bio-AFM: Nanowizard 4 (JPK instruments). The measurements were conducted using the DNP-S10 (Bruker) chip. A V-shaped cantilever B with a nominal spring constant of 0.06 N/m and a nominal radius of curvature of 10 nm was employed. High-resolution images were captured using the specialized Quantitative Imaging (QI) mode, enabling the acquisition of mechanical properties at each scanned pixel. Large-scale force maps were obtained in the contact mode, with setpoints ranging from 2 to 5 nN. The AFM instrument was mounted on top of an inverted microscope (Zeiss) to aid tissue localization. Additionally, an in-house built incubator enveloped the AFM, creating an environment of 37°C and 5% CO₂. This setup allowed for extended measurements without compromising cell conditions. Data acquisition and processing were performed with the JPKSPM software version 6.1.165 (JPK BioAFM, Bruker, <https://www.jpk.com/>). The Young's modulus was computed using the Hertz/Sneddon model adjusted for parabolic indenters [42-44], based on force curves. Following Young's modulus calculation, the elasticity data underwent normalization and filtering in MATLAB version R2019b Update 6. The perinuclear area was defined based on the height maps to specifically determine the stiffness of the perinuclear area.

Statistical analysis

SPSS statistics version 23.0 for Windows (IBM Corp) was used for statistical analysis. Statistical comparisons were conducted through an unpaired t-test, and the results were presented as a two-tailed p-value to assess the significance of differences between two independent means, with a significance level set at 0.05. GraphPad Prism software for Windows was used to generate graphs.

Funding

J.v.H. and her research is supported by Special Research Fund of Ghent University (BOF19/24J/139). S.S. is supported by BHF awards FS/18/46/33663 and RG/17/5/32936. A.G.S. acknowledges support of FWO (1002620N) and Special Research Fund of Ghent University (BOF/IOP/2022/033).

Acknowledgements

The authors thank Natasja Van den Vreken and Marleen De Groote for their technical support. We are also grateful for the help of Lisa Dangreau and Jasmine Beeckman for setting up cardiac fibroblast differentiations and optimizing 3D co-cultures.

Author contributions

J.A. and J.v.H. conceived the study and designed experiments; J.A., L.L. and L.V.d.M. performed the experiments; J.A., L.L., L.V.d.M. and J.v.H. performed interpretation of data, J.A., L.L. and J.v.H. drafted the paper, L.V.d.M., S.S., A.G.S., J.D.B. conducted review and revisions; J.v.H. contributed to the design and provided resources. All authors approved the final version of the manuscript.

Declaration of interest

The authors have no competing interests related to this work.

References

- [1] K. Asano, A. Cantalupo, L. Sedes, F. Ramirez, The Multiple Functions of Fibrillin-1 Microfibrils in Organismal Physiology, *Int. J. Mol. Sci.* 23(3) (2022).
- [2] K.A. Zeyer, D.P. Reinhardt, Fibrillin-containing microfibrils are key signal relay stations for cell function, *J Cell Commun Signal* 9(4) (2015) 309-25.
- [3] Z.X. Chen, W.N. Jia, Y.X. Jiang, Genotype-phenotype correlations of marfan syndrome and related fibrillinopathies: Phenomenon and molecular relevance, *Front Genet* 13 (2022) 943083.
- [4] D.M. Milewicz, A.C. Braverman, J. De Backer, S.A. Morris, C. Boileau, I.H. Maumenee, G. Jondeau, A. Evangelista, R.E. Pyeritz, Marfan syndrome, *Nat Rev Dis Primers* 7(1) (2021) 64.
- [5] R.E. Pyeritz, Marfan syndrome: improved clinical history results in expanded natural history, *Genet. Med.* 21(8) (2019) 1683-1690.
- [6] F. Alpendurada, J. Wong, A. Kiotsekoglou, W. Banya, A. Child, S.K. Prasad, D.J. Pennell, R.H. Mohiaddin, Evidence for Marfan cardiomyopathy, *Eur. J. Heart Fail.* 12(10) (2010) 1085-91.
- [7] R. Hetzer, G. Siegel, E.M. Delmo Walter, Cardiomyopathy in Marfan syndrome, *Eur. J. Cardiothorac. Surg.* 49(2) (2016) 561-8.
- [8] A.T. Yetman, R.A. Bornemeier, B.W. McCrindle, Long-term outcome in patients with Marfan syndrome: is aortic dissection the only cause of sudden death?, *J. Am. Coll. Cardiol.* 41(2) (2003) 329-32.
- [9] A. Demolder, Y. von Kodolitsch, L. Muiño-Mosquera, J. De Backer, Myocardial Function, Heart Failure and Arrhythmia in Marfan Syndrome: A Systematic Literature Review, *Diagnostics* 10(10) (2020).
- [10] J. Aalders, L. Léger, L. Van der Meeren, N. Van den Vreken, A.G. Skirtach, S. Sinha, J. De Backer, J. van Hengel, Effects of fibrillin mutations on the behavior of heart muscle cells in Marfan syndrome, *Sci. Rep.* 10(1) (2020) 16756.
- [11] C.O. Heras-Bautista, N. Mikhael, J. Lam, V. Shinde, A. Katsen-Globa, S. Dieluweit, M. Molcanyi, V. Uvarov, P. Jütten, R.G.A. Sahito, F. Mederos-Henry, A. Piechot, K. Brockmeier, J. Hescheler, A. Sachinidis, K. Pfannkuche, Cardiomyocytes facing fibrotic conditions re-express extracellular matrix transcripts, *Acta Biomater.* 89 (2019) 180-192.
- [12] P. Zhou, W.T. Pu, Recounting Cardiac Cellular Composition, *Circ. Res.* 118(3) (2016) 368-70.
- [13] O. Bergmann, S. Zdunek, A. Felker, M. Salehpour, K. Alkass, S. Bernard, S.L. Sjöstrom, M. Szewczykowska, T. Jackowska, C. Dos Remedios, T. Malm, M. Andrä, R. Jashari, J.R. Nyengaard, G. Possnert, S. Jovinge, H. Druid, J. Frisé, Dynamics of Cell Generation and Turnover in the Human Heart, *Cell* 161(7) (2015) 1566-75.

- [14] K. Breckwoldt, D. Letuffe-Brenière, I. Mannhardt, T. Schulze, B. Ulmer, T. Werner, A. Benzin, B. Klampe, M.C. Reinsch, S. Laufer, A. Shibamiya, M. Prondzynski, G. Mearini, D. Schade, S. Fuchs, C. Neuber, E. Krämer, U. Saleem, M.L. Schulze, M.L. Rodriguez, T. Eschenhagen, A. Hansen, Differentiation of cardiomyocytes and generation of human engineered heart tissue, *Nat. Protoc.* 12(6) (2017) 1177-1197.
- [15] E. Giacomelli, M. Bellin, L. Sala, B.J. van Meer, L.G.J. Tertoolen, V.V. Orlova, C.L. Mummery, Three-dimensional cardiac microtissues composed of cardiomyocytes and endothelial cells co-differentiated from human pluripotent stem cells, *Development* (2017) 143438.
- [16] J. Aalders, L. Léger, T. Tuerlings, S. Ledda, J. van Hengel, Liquid marble technology to create cost-effective 3D cardiospheres as a platform for in vitro drug testing and disease modelling, *MethodsX* 7 (2020) 101065.
- [17] P. Beauchamp, C.B. Jackson, L.C. Ozhathil, I. Agarkova, C.L. Galindo, D.B. Sawyer, T.M. Suter, C. Zuppinger, 3D Co-culture of hiPSC-Derived Cardiomyocytes With Cardiac Fibroblasts Improves Tissue-Like Features of Cardiac Spheroids, *Front Mol Biosci* 7 (2020) 14.
- [18] A. Granata, F. Serrano, W.G. Bernard, M. McNamara, L. Low, P. Sastry, S. Sinha, An iPSC-derived vascular model of Marfan syndrome identifies key mediators of smooth muscle cell death, *Nat. Genet.* 49(1) (2017) 97-109.
- [19] A. Kahn-Krell, D. Pretorius, B. Guragain, X. Lou, Y. Wei, J. Zhang, A. Qiao, Y. Nakada, T.J. Kamp, L. Ye, J. Zhang, A three-dimensional culture system for generating cardiac spheroids composed of cardiomyocytes, endothelial cells, smooth-muscle cells, and cardiac fibroblasts derived from human induced-pluripotent stem cells, *Front. bioeng. biotechnol.* 10 (2022) 908848.
- [20] E. Giacomelli, V. Meraviglia, G. Campostrini, A. Cochrane, X. Cao, R.W.J. van Helden, A. Krotenberg Garcia, M. Mircea, S. Kostidis, R.P. Davis, B.J. van Meer, C.R. Jost, A.J. Koster, H. Mei, D.G. Míguez, A.A. Mulder, M. Ledesma-Terrón, G. Pompilio, L. Sala, D.C.F. Salvatori, R.C. Slieker, E. Sommariva, A.A.F. de Vries, M. Giera, S. Semrau, L.G.J. Tertoolen, V.V. Orlova, M. Bellin, C.L. Mummery, Human-iPSC-Derived Cardiac Stromal Cells Enhance Maturation in 3D Cardiac Microtissues and Reveal Non-cardiomyocyte Contributions to Heart Disease, *Cell stem cell* 26(6) (2020) 862-879.
- [21] M.O. Lee, K.B. Jung, S.J. Jo, S.A. Hyun, K.S. Moon, J.W. Seo, S.H. Kim, M.Y. Son, Modelling cardiac fibrosis using three-dimensional cardiac microtissues derived from human embryonic stem cells, *J. Biol. Eng.* 13 (2019) 15.
- [22] S.M. Biendarra-Tiegs, D.J. Clemens, F.J. Secreto, T.J. Nelson, Human Induced Pluripotent Stem Cell-Derived Non-Cardiomyocytes Modulate Cardiac Electrophysiological Maturation Through Connexin 43-Mediated Cell-Cell Interactions, *Stem Cells Dev.* 29(2) (2020) 75-89.
- [23] J.R. Cook, L. Carta, L. Bénard, E.R. Chemaly, E. Chiu, S.K. Rao, T.G. Hampton, P. Yurchenco, K.D. Costa, R.J. Hajjar, F. Ramirez, Abnormal muscle mechanosignaling triggers cardiomyopathy in mice with Marfan syndrome, *J. Clin. Invest.* 124(3) (2014) 1329-39.
- [24] C.K. Nagaraju, E. Dries, G. Gilbert, M. Abdesselem, N. Wang, M. Amoni, R.B. Driesen, K.R. Sipido, Myofibroblast modulation of cardiac myocyte structure and function, *Sci. Rep.* 9(1) (2019) 8879.
- [25] F. Schultz, P. Swiatlowska, A. Alvarez-Laviada, J.L. Sanchez-Alonso, Q. Song, A.A.F. de Vries, D.A. Pijnappels, E. Ongstad, V.M.M. Braga, E. Entcheva, R.G. Gourdie, M. Miragoli, J. Gorelik, Cardiomyocyte-myofibroblast contact dynamism is modulated by connexin-43, *FASEB J.* 33(9) (2019) 10453-10468.
- [26] L. Leybaert, M.A. De Smet, A. Lissoni, R. Allewaert, H.L. Roderick, G. Bultynck, M. Delmar, K.R. Sipido, K. Witschas, Connexin hemichannels as candidate targets for cardioprotective and anti-arrhythmic treatments, *J. Clin. Invest.* 133(6) (2023).
- [27] J.W. Smyth, R.M. Shaw, Autoregulation of connexin43 gap junction formation by internally translated isoforms, *Cell Rep.* 5(3) (2013) 611-8.
- [28] M. Miragoli, G. Gaudesius, S. Rohr, Electrotonic modulation of cardiac impulse conduction by myofibroblasts, *Circ. Res.* 98(6) (2006) 801-10.

- [29] T.R. Brown, T. Krogh-Madsen, D.J. Christini, Illuminating Myocyte-Fibroblast Homotypic and Heterotypic Gap Junction Dynamics Using Dynamic Clamp, *Biophys. J.* 111(4) (2016) 785-797.
- [30] F.B. Bedada, S.S. Chan, S.K. Metzger, L. Zhang, J. Zhang, D.J. Garry, T.J. Kamp, M. Kyba, J.M. Metzger, Acquisition of a quantitative, stoichiometrically conserved ratiometric marker of maturation status in stem cell-derived cardiac myocytes, *Stem Cell Rep.* 3(4) (2014) 594-605.
- [31] K. Perepelina, A. Zaytseva, A. Khudiakov, I. Neganova, E. Vasichkina, A. Malashicheva, A. Kostareva, LMNA mutation leads to cardiac sodium channel dysfunction in the Emery-Dreifuss muscular dystrophy patient, *Front Cardiovasc Med* 9 (2022) 932956.
- [32] E.T. Hoorntje, I.A. Bollen, D.Q. Barge-Schaapveld, F.H. van Tienen, G.J. Te Meerman, J.A. Jansweijer, A.J. van Essen, P.G. Volders, A.A. Constantinescu, P.C. van den Akker, K.Y. van Spaendonck-Zwarts, R.A. Oldenburg, C.L. Marcelis, J.J. van der Smagt, E.A. Hennekam, A. Vink, M. Bootsma, E. Aten, A.A. Wilde, A. van den Wijngaard, J.L. Broers, J.D. Jongbloed, J. van der Velden, M.P. van den Berg, J.P. van Tintelen, Lamin A/C-Related Cardiac Disease: Late Onset With a Variable and Mild Phenotype in a Large Cohort of Patients With the Lamin A/C p.(Arg331Gln) Founder Mutation, *Circ. Cardiovasc. Genet.* 10(4) (2017).
- [33] N.Y. Chen, P. Kim, T.A. Weston, L. Edillo, Y. Tu, L.G. Fong, S.G. Young, Fibroblasts lacking nuclear lamins do not have nuclear blebs or protrusions but nevertheless have frequent nuclear membrane ruptures, *Proc. Natl. Acad. Sci. U. S. A.* 115(40) (2018) 10100-10105.
- [34] A.D. Stephens, P.Z. Liu, E.J. Banigan, L.M. Almassalha, V. Backman, S.A. Adam, R.D. Goldman, J.F. Marko, Chromatin histone modifications and rigidity affect nuclear morphology independent of lamins, *Mol. Biol. Cell* 29(2) (2018) 220-233.
- [35] Y.H. Chi, W.P. Wang, M.C. Hung, G.G. Liou, J.Y. Wang, P.G. Chao, Deformation of the nucleus by TGF β 1 via the remodeling of nuclear envelope and histone isoforms, *Epigenetics Chromatin* 15(1) (2022) 1.
- [36] C. Tamiello, M.A. Kamps, A. van den Wijngaard, V.L. Verstraeten, F.P. Baaijens, J.L. Broers, C.C. Bouten, Soft substrates normalize nuclear morphology and prevent nuclear rupture in fibroblasts from a laminopathy patient with compound heterozygous LMNA mutations, *Nucleus (Calcutta)* 4(1) (2013) 61-73.
- [37] J. Aalders, N. Van den Vreken, M. Popovic, S. Mishra, B. Heindryckx, J. van Hengel, Robust protocol for feeder-free adaptation of cryopreserved human pluripotent stem cells, *In Vitro Cell Dev. Biol. Anim.* 55(10) (2019) 777-783.
- [38] P.W. Burridge, E. Matsa, P. Shukla, Z.C. Lin, J.M. Churko, A.D. Ebert, F. Lan, S. Diecke, B. Huber, N.M. Mordwinkin, J.R. Plews, O.J. Abilez, B. Cui, J.D. Gold, J.C. Wu, Chemically defined generation of human cardiomyocytes, *Nat. Methods* 11(8) (2014) 855-60.
- [39] J. Schindelin, I. Arganda-Carreras, E. Frise, V. Kaynig, M. Longair, T. Pietzsch, S. Preibisch, C. Rueden, S. Saalfeld, B. Schmid, J.-Y. Tinevez, D.J. White, V. Hartenstein, K. Eliceiri, P. Tomancak, A. Cardona, Fiji: an open-source platform for biological-image analysis, *Nat. Methods* 9(7) (2012) 676-682.
- [40] J.E. Saffitz, K.G. Green, W.J. Kraft, K.B. Schechtman, K.A. Yamada, Effects of diminished expression of connexin43 on gap junction number and size in ventricular myocardium, *Am. J. Physiol. Heart Circ. Physiol.* 278(5) (2000) H1662-70.
- [41] J. Vandesompele, K. De Preter, F. Pattyn, B. Poppe, N. Van Roy, A. De Paepe, F. Speleman, Accurate normalization of real-time quantitative RT-PCR data by geometric averaging of multiple internal control genes, *Genome Biol.* 3(7) (2002).
- [42] I.N. Sneddon, The relation between load and penetration in the axisymmetric boussinesq problem for a punch of arbitrary profile, *Int. J. Eng. Sci.* 3(1) (1965) 47-57.
- [43] JPKinstruments, Determining the elastic modulus of biological samples using atomic force microscopy., Available at: <https://www.jpk.com/app-technotes-img/AFM/pdf/jpk-app-elastic-modulus.14-1.pdf>. (Accessed: 16th December 2019) (2014) 1–9

[44] L. Van der Meeren, J. Verduijn, D.V. Krysko, A.G. Skirtach, AFM Analysis Enables Differentiation between Apoptosis, Necroptosis, and Ferroptosis in Murine Cancer Cells, *iScience* 23(12) (2020) 101816.

Figure legends:

Figure 1. Schematic overview of the study approach. **(A)** iPSCs are differentiated into cardiomyocytes (CM) and cardiac fibroblasts (CF). **(B)** To generate cardiospheres 85% CMs (14 day-old) are mixed with 15% CFs (30 day-old) and seeded on low-attachment plates for self-assembly. **(C)** After 7 days of cardiosphere culture, the structures are dissociated and seeded on Geltrex coated glass coverslips. **(A)** Nuclear blebbing is assessed in iPSC derived CMs and CFs separately. Atomic force microscopy (AFM) is performed on the iPSC derived CFs. **(B)** After 7 days of cardiosphere culture size and shape of the cells was measured, also cells were collected for gene expression analysis. **(C)** Sarcomere length and binucleation of CMs was analysed on 2D monolayers from dissociated cardiospheres. CX43 gap junction formation was determined using immunostaining for connexin-43.

Figure 2. Characteristics of cardiospheres. **(A)** Representative phase-contrast images of cardiospheres at different days culture. Scalebar, 500 μm . **(B)** Quantification of average diameter and circularity of cardiospheres from 1 day-old to 21 day-old cardiospheres. **(C)** Gene expression analysis for 7 day-, 14 day- and 21 day-old cardiospheres for *FBN1*, *GJA1*, *TNNT2*, *TNNI1* and *TNNI3*. Blue indicates a low gene expression, red indicates a high gene expression, expressed as normalized expression. **(D)** Average diameter of 7 day-old cardiospheres from 6 independent experiments, at least 10 cardiospheres per replicate were analysed. Corrected cardiomyocytes (Cor CM, black dots) or Marfan cardiomyocytes (MFS CM, red dots), co-cultured with corrected cardiac fibroblast (Cor CF) or Marfan cardiac fibroblasts (MFS CF). **(E)** Mean fluorescent intensity of Hoechst signal for pooled corrected cardiomyocyte containing cardiospheres (black dots) and pooled for Marfan cardiomyocyte cardiospheres (red dots) at different days. **(F)** Integrated density of Hoechst fluorescence for corrected cardiospheres (black dots) and Marfan cardiospheres (red dots) at different days. Asterisks indicate significance level: * $p < 0.05$; ** $p < 0.01$; *** $p < 0.001$.

Figure 3. Gene expression analysis of cardiospheres. Gene expression for *FBN1*, *GJA1*, *MLC2v*, *MLC2a*, *ITGB1*, *COL1A2*, *TNNT2*, *TNNI3* and *TNNI1* was evaluated for pooled cardiospheres (5-10 per condition). Gene expression was normalized by reference genes *B2M* and *RPL13A* and presented as the average of 3 independent experiments. The cardiospheres with MFS CMs (red dots) are compared with the cardiospheres containing Cor CMs (black dots). Error bars indicate standard error. Asterisks indicate significance level: * $p < 0.05$; ** $p < 0.01$.

Figure 4. Representative confocal images of cadherin, β -catenin and connexin-43 at the cell-cell border. Cardiospheres were dissociated for immunohistochemical analysis in 2D monolayer. Coupling of cardiomyocytes of both corrected and Marfan revealed by immunohistochemical staining for **(A)** pan-cadherin (red), **(B)** β -catenin (red) or **(C)** connexin-43 (red) and counterstained with α -actinin (green) and Hoechst (blue). Arrowheads point to the specific connecting structure (cadherin, β -catenin and connexin-43) at the cell-cell borders. **(A)** Cadherin localization at the cell-cell borders of corrected cardiomyocytes (Cor CM) or Marfan cardiomyocytes (MFS CM). A magnified image is also shown, the area of magnification is indicated with the white square. **(B)** β -catenin localization at the cell-cell borders of Cor CM or MFS CM. **(C)** Connexin-43 localization at the cell-cell border of Cor CM, MFS CM and the interaction with CFs, CMs were co-cultured with corrected cardiac fibroblast (Cor CF) or Marfan cardiac fibroblasts (MFS CF) in cardiospheres. Coupling between cardiac fibroblasts and cardiomyocytes was shown for connexin-43. The location of the cardiomyocyte and cardiac fibroblast is indicated in the magnified image of the co-cultured cardiospheres by respectively CM and CF. Scalebars, 10 μm .

Figure 5. Analysis of structural properties of cardiomyocytes and cardiac fibroblast for co-culture experiments for corrected cardiomyocytes (Cor CM), Marfan cardiomyocytes (MFS CM), corrected cardiac fibroblasts (Cor CF) and Marfan cardiac fibroblasts (MFS CF). **(A)** Confocal image of representative cardiomyocytes derived from 3D cultures of cardiospheres stained for α -actinin (green) and nucleus (Hoechst, blue). The arrow in the magnified image shows the distance between two z-bands, which indicates the sarcomere length. Scalebar, 20 μm in left image, 2 μm in magnified image. **(B)** Average sarcomere length of cardiomyocytes from 4 independent experiments (between 61-77 cardiomyocytes measured for each condition). Error bars indicate standard error. **(C)** Confocal image of cardiomyocytes in monolayer that underwent 3D culture in cardiospheres stained for α -actinin (green), NKX2.5 (red) and nucleus (Hoechst, blue). Arrow points to binucleated cardiomyocytes. Scalebar, 50 μm . **(D)** Mononucleated cardiomyocytes have a single nucleus while binucleated cardiomyocytes have two. **(E)** Average percentage of binucleated cardiomyocytes in cardiospheres for 4 independent experiments. Error bars indicate standard error. **(F)** Confocal images of representative images of Cor CFs and MFS CFs stained for DDR2 (green), Lamin A/C (red) and nucleus (Hoechst, blue). Arrow points to a nuclear bleb. Scalebar, 20 μm . **(G)** Confocal image of MFS CMs stained for α -actinin (green), Lamin A/C (red) and nucleus (Hoechst, blue). Arrow points to a nuclear protrusion. Scalebar, 10 μm . **(H)** Average percentage of nuclei with protrusions of Cor CM,

MFS CM, Cor CF, and MFS CF. 8-15 representative regions of 475 μm by 350 μm per condition, containing in total at least 100 nuclei, were analysed from 2 independent experiments. Error bars indicate standard error. **(I)** Atomic force microscope images of Cor CFs and MFS CFs. Mechanical stiffness mapping is overlaid with topography mapping. The dimensions are indicated in μm . A blue colour indicates a low Young's Modulus, while a red colour indicates high Young's Modulus. The yellow arrows indicate the nuclear area of a complete CF. **(J)** The average Young's Modulus of CFs from 2 independent experiments was measured with atomic force microscopy for 4 areas of 200 μm by 200 μm , containing respectively 16 Cor CFs and 14 MFS CFs. The graphs show the results for the peri-nuclear area. Error bars indicate standard error. Asterisks indicate significance level: * $p < 0.05$; ** $p < 0.01$; *** $p < 0.001$.

Figure 1

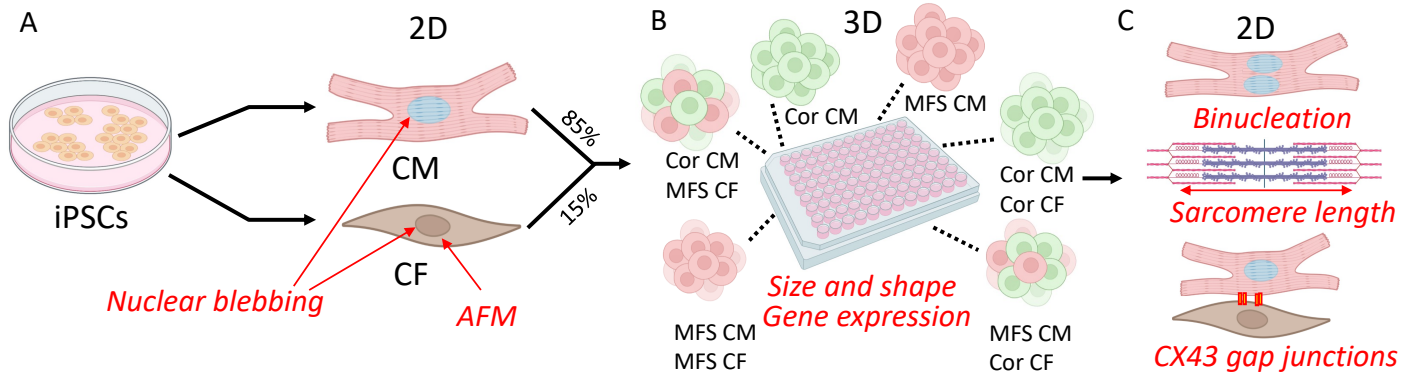


Figure 2

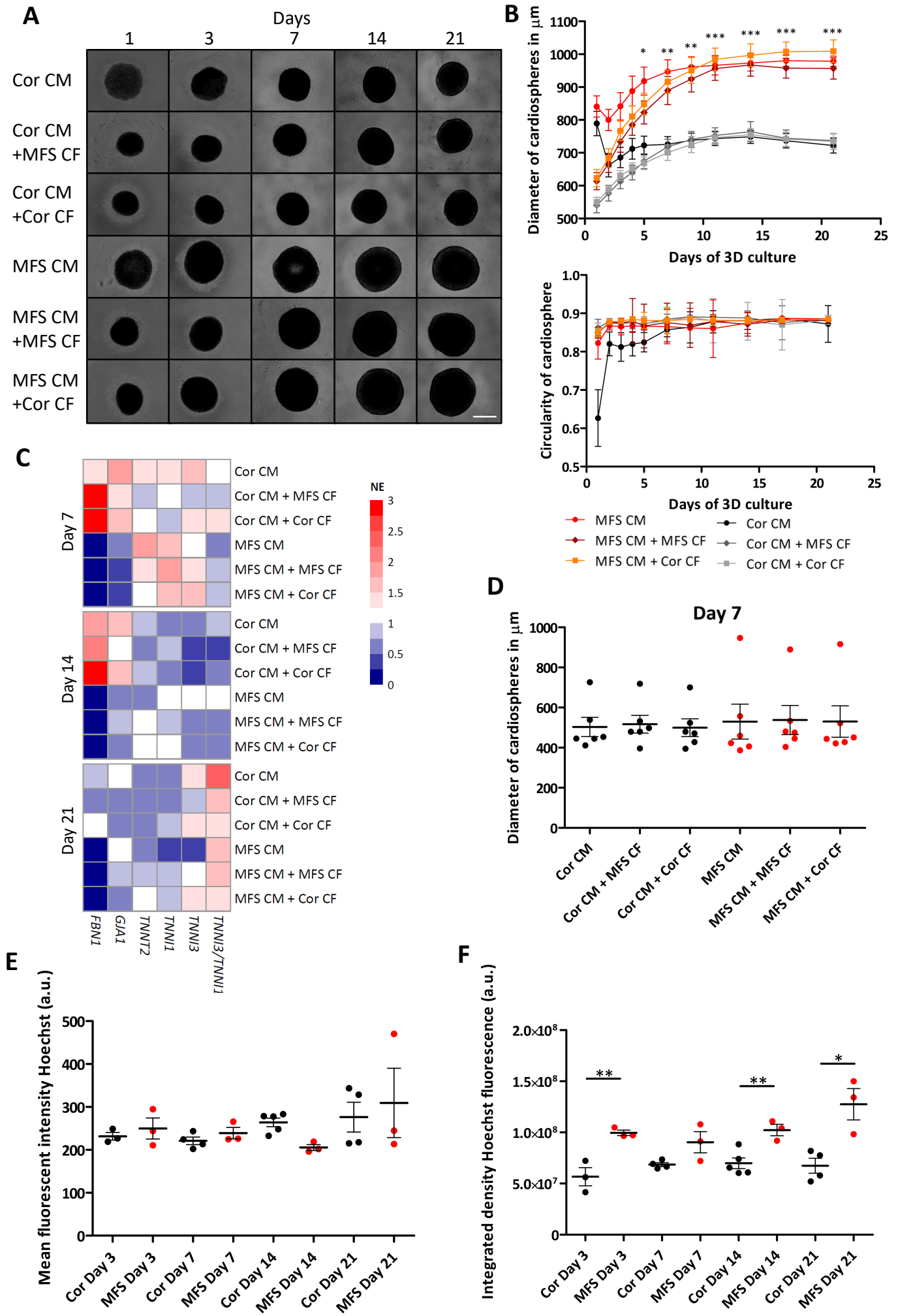


Figure 3

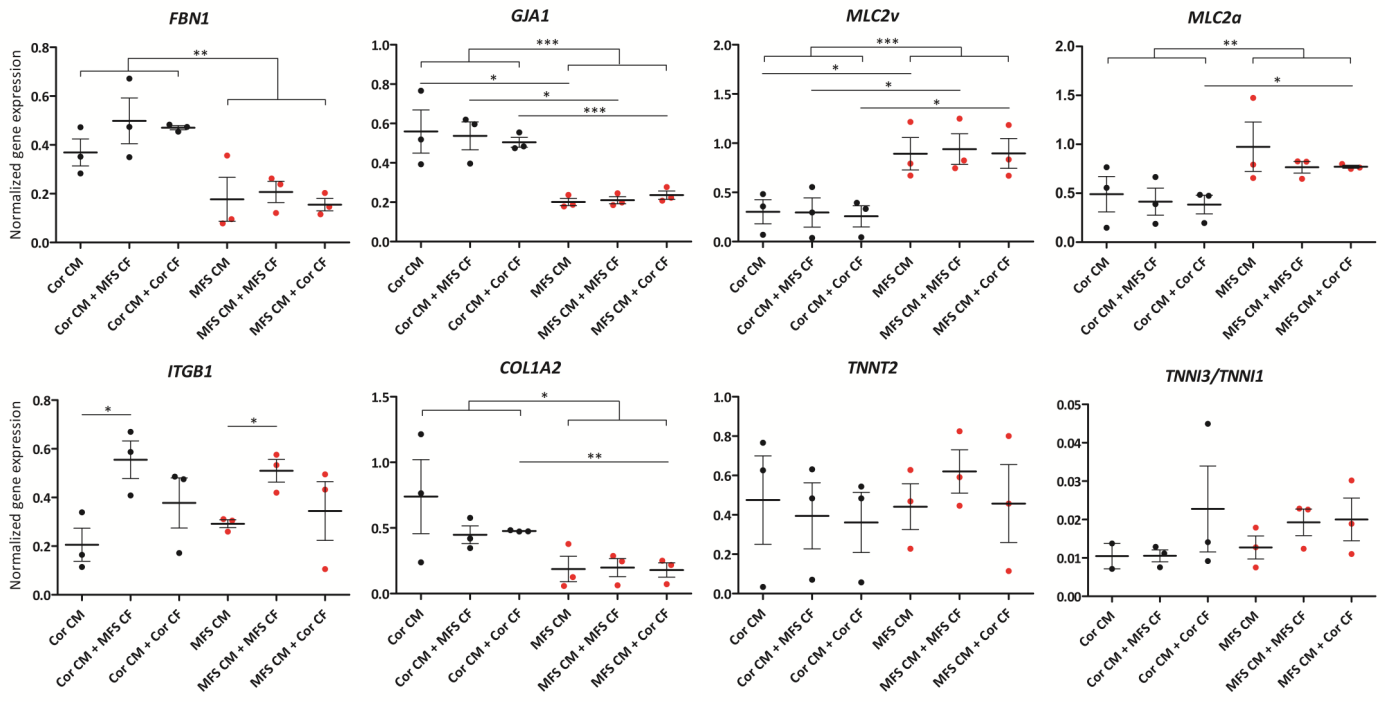


Figure 4

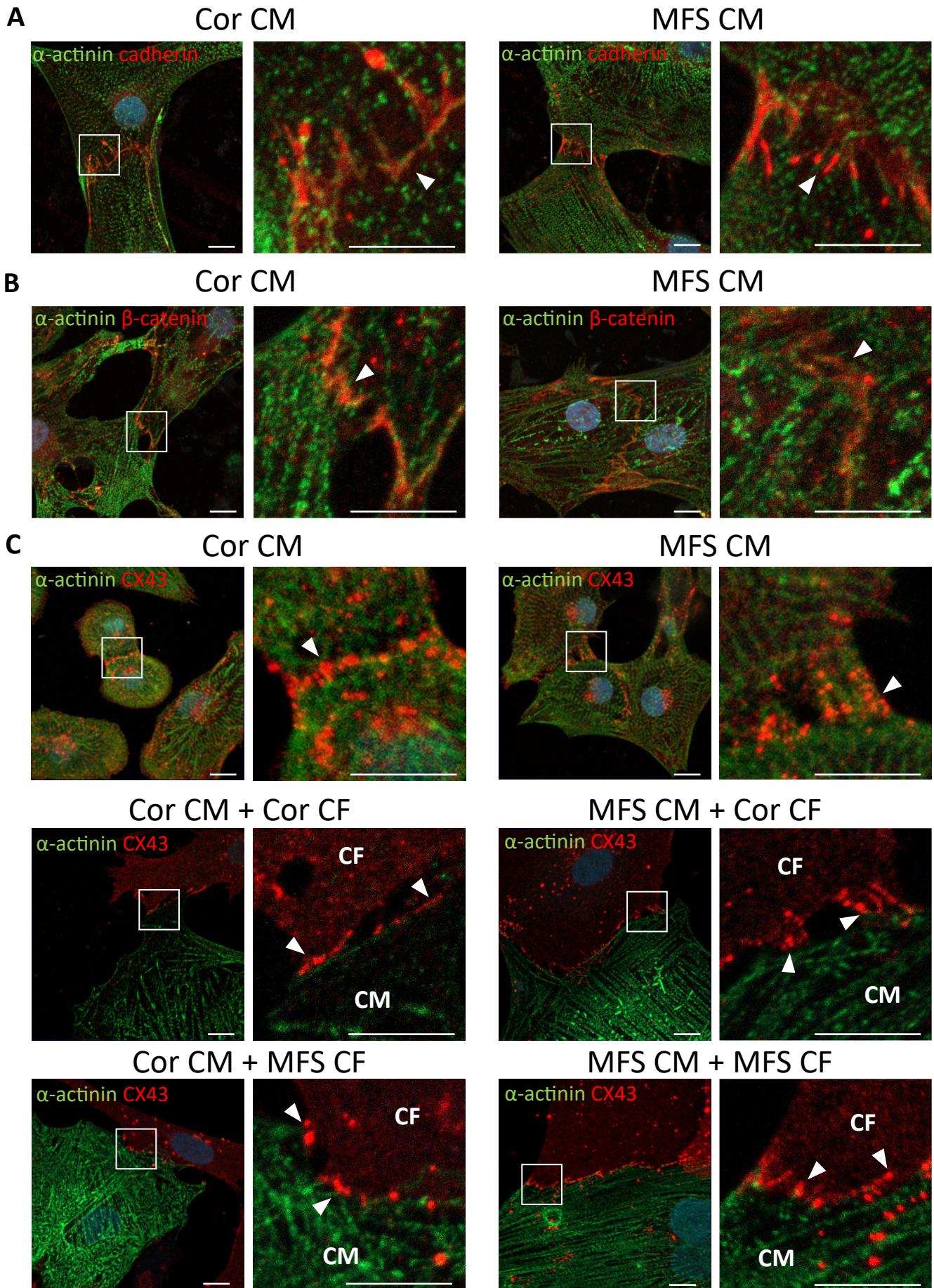
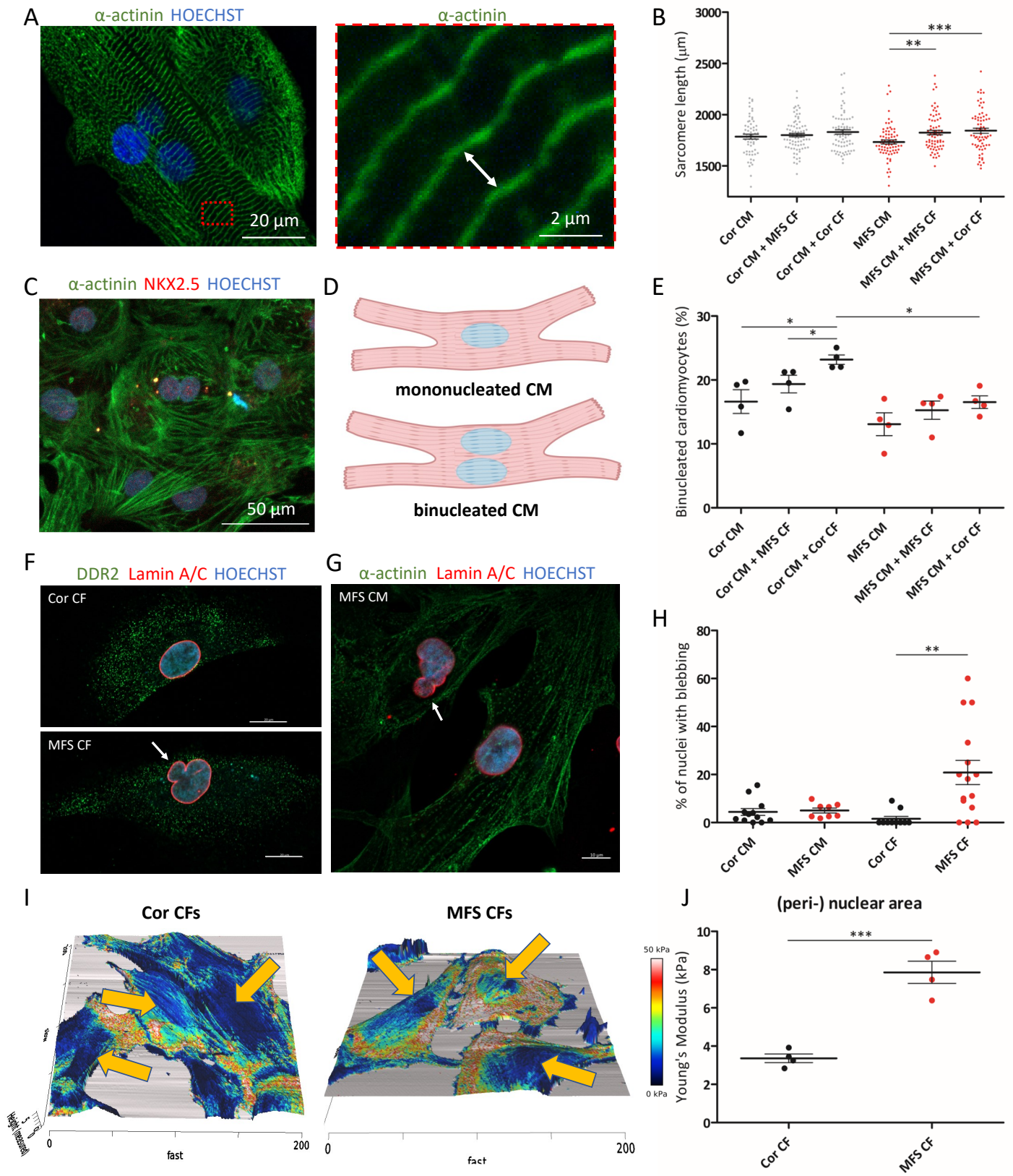
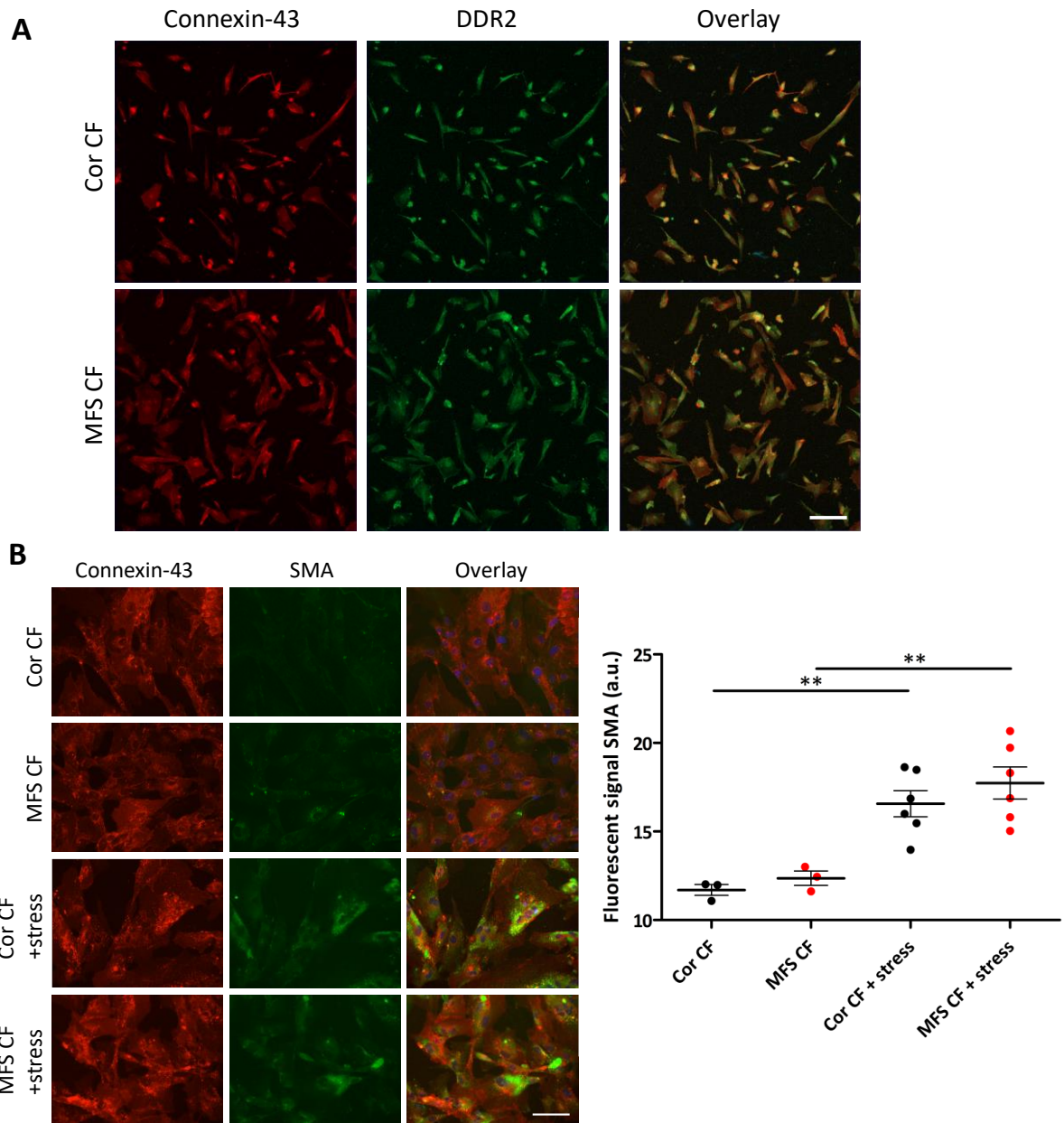
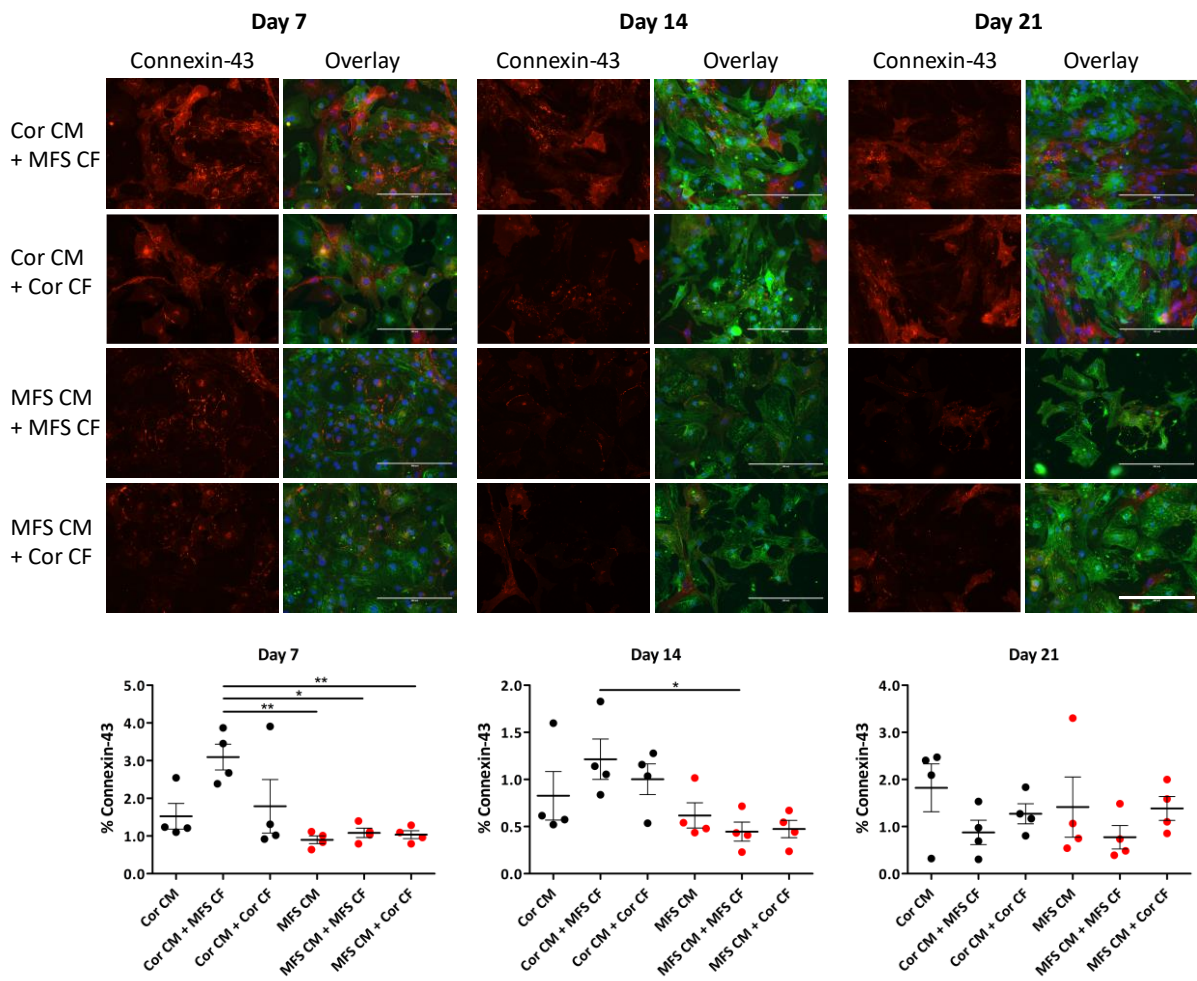


Figure 5

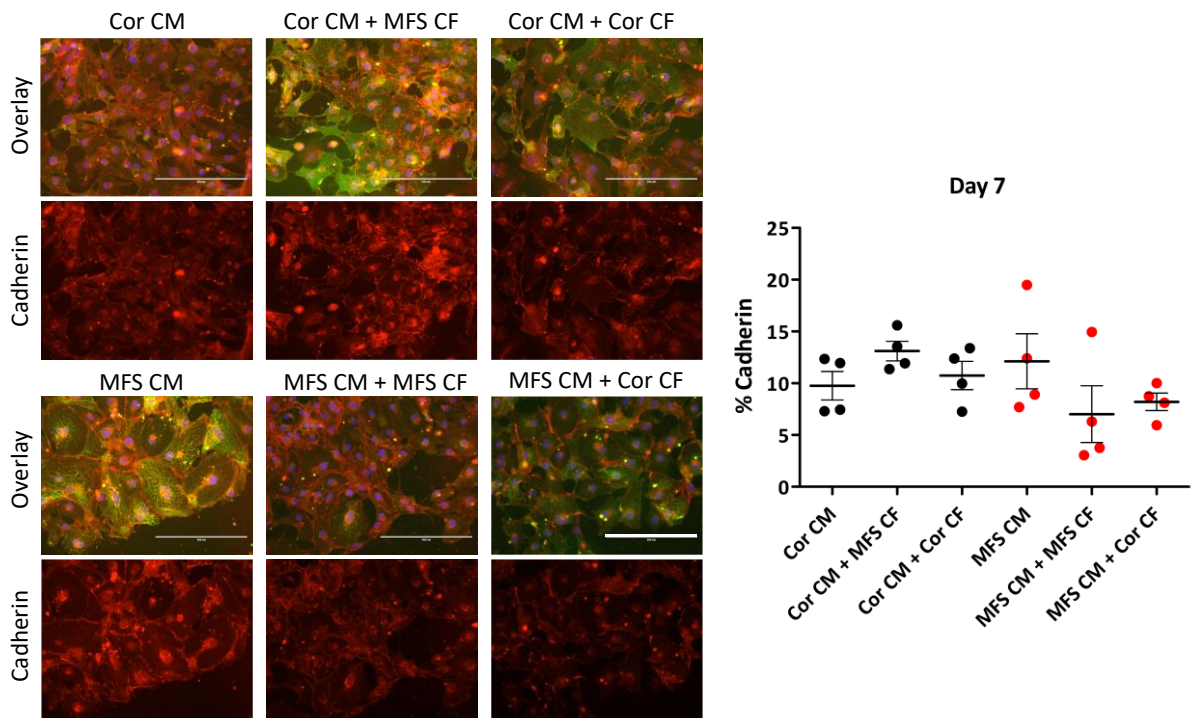




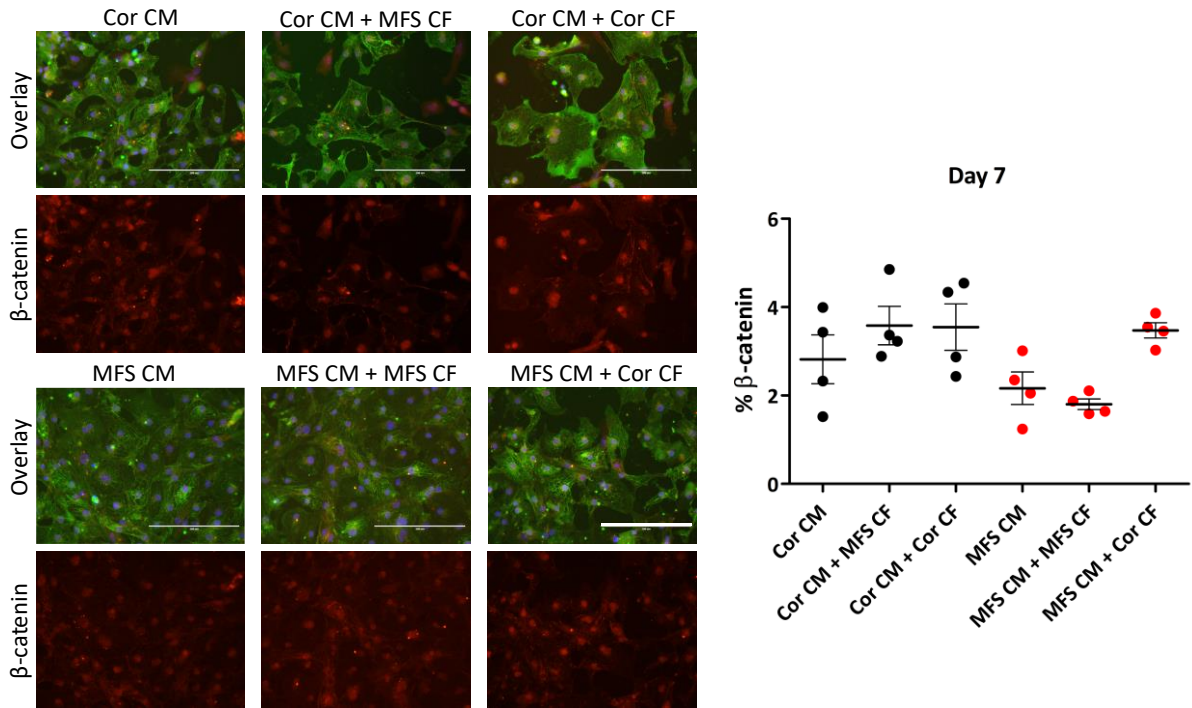
Supplementary Figure 1. Characterization of quiescent cardiac fibroblasts. **(A)** Both corrected cardiac fibroblasts (Cor CF) and Marfan cardiac fibroblasts (MFS CF) display expression of connexin-43 (red) and DDR2 (green), typical CF markers. Scalebar, 200 μ m. **(B)** Immunofluorescent analysis of smooth muscle actin (SMA) expression in CF exposed to stress by increased culture confluency for 7 days compared to control CF. Scalebar, 200 μ m. Quantification of fluorescent SMA signal is displayed. Asterisks indicate significance level: ** $p < 0.01$.



Supplementary Figure 2. Immunofluorescent analysis of connexin-43 abundance in 7 day-, 14 day- and 21 day-old cardiospheres. Representative images were provided, The red signal in the fluorescent images represents connexin-43, in the overlay α -actinin (green) and Hoechst (blue) is added. Scalebar, 200 μ m. Quantification of connexin-43 abundance is performed on 4 randomly selected images and presented in % of the cell area that is positive for positive connexin-43 staining. Asterisks indicate significance level: * p<0.05; ** p<0.01.



Supplementary Figure 3. Immunofluorescent analysis of cadherin abundance in 7 day-old cardiospheres. The pan-cadherin antibody visualize most probably N-cadherin. Representative images were provided, The red signal in the fluorescent images represents pan-cadherin, in the overlay α -actinin (green) and Hoechst (blue) is added. Scalebar, 200 μ m. Quantification of cadherin abundance is performed on 4 randomly selected images and presented in % of the cell area that is positive for positive pan-cadherin staining.



Supplementary Figure 4. Immunofluorescent analysis of β -catenin abundance in 7 day-old cardiospheres. Representative images were provided, The red signal in the fluorescent images represents β -catenin, in the overlay α -actinin (green) and Hoechst (blue) is added. Scalebar, 200 μ m. Quantification of β -catenin abundance is performed on 4 randomly selected images and presented in % of the cell area that is positive for positive β -catenin staining.

Supplementary table 1. Antibodies used for immunostaining.

Antibody	Dilution	Company	Cat No.
α -actinin mouse mAb (IgG1)	1/800	Merck	A7811
NKX2.5 rabbit Ab	1/100	Life technologies	701622
DDR2 mouse mAb	1/100	Santa Cruz Biotechnology	sc-81707
Lamin A/C rabbit mAb (IgG1)	1/250	Abcam	ab108595
CX43 rabbit Ab	1/4000	Sigma	C6219
Pan-cadherin rabbit Ab	1/500	Sigma	C3678
β -catenin rabbit Ab	1/2000	Sigma	C2206
α -smooth muscle actin mouse mAb	1/200	Fisher Scientific	11324473
goat-anti-mouse IgG dylight 488	1/500	Life Technologies	35503
goat-anti-mouse IgG dylight 594	1/500	Life Technologies	35511
goat-anti-rabbit IgG dylight 488	1/500	Life Technologies	35553
goat-anti-rabbit IgG dylight 594	1/500	Life Technologies	35561

Supplementary table 2. Primers used in RT-qPCR.

Target	Forward primer	Reverse primer
<i>B2M</i>	5'-TGCTGTCTCCATGTTTGATGTATCT-3'	5'-TCTCTGCTCCCCACCTCTAAGT-3'
<i>RPL13A</i>	5'-CCTGGAGGAGAAGAGGAAAGAGA-3'	5'-TTGAGGACCTCTGTGTATTTGTCAA-3'
<i>FBN1</i>	5'-ACCGTGCTTTTAGCGTCCTA-3'	5'-GGCAAATGGGGACAATACAC-3'
<i>GJA1</i>	5'-TCTGAGTGCCTGAACTTGCC-3'	5'-CCCTCCAGCAGTTGAGTAGG-3'
<i>MLC2v</i>	5'-GAAGGCTGATTACGTTCCGGG-3'	5'-CCTTCTCTTCTCCGTGGGTG-3'
<i>MLC2a</i>	5'-CCGTCTTCCTCACGCTCTTT-3'	5'-AACATCTGCTCCACCTCAGC-3'
<i>ITGB1</i>	5'-GCCGCGCGGAAAAGATGAAT-3'	5'-TGCTGTTCCCTTTGCTACGGT-3'
<i>COL1A2</i>	5'-CCTGGCAATATTGGTCCCGT-3'	5'-ACCATGGTGACCAGCGATAC-3'
<i>TNNT2</i>	5'-TTCACCAAAGATCTGCTCCTCGCT-3'	5'-TTACTACTGGTGTGGAGTGGGTGG-3'
<i>TNNI1</i>	5'-TGGATGAGGAGCGATACGAC-3'	5'-TTGTGAGGTCGGAGACTTGG-3'
<i>TNNI3</i>	5'-CGATGCGGCTAGGGAACCTC-3'	5'-TGCAATTTTCTCGAGGCGGA-3'